Polymer 210 (2020) 122995

Contents lists available at ScienceDirect

Polymer

journal homepage: http://www.elsevier.com/locate/polymer

The dissociation of physical interaction clusters under tensile deformation of hybrid double network gels

Ruiqi Zhao, Yu Wang **, Sheng Wang, Chunyu Zhao, Xinglong Gong *

CAS Key Laboratory of Mechanical Behavior and Design of Materials, Department of Modern Mechanics, CAS Center for Excellence in Complex System Mechanics, University of Science and Technology of China, Hefei, Anhui, 230027, People's Republic of China

ARTICLE INFO

Keywords:
Hybrid double network gels
Coarse-grained molecular dynamics simulation
Rate-dependent behavior

ABSTRACT

Hybrid double network (DN) gels, including the physical interaction (PI) network and chemically cross-linked (C-CL) network, exhibit superior mechanical behaviors. Herein, the influence of the physical interaction strength and the strain rate on mechanical properties of hybrid DN gels was investigated by exploiting coarse-grained molecular dynamics simulations. The PI network was constructed successfully based on clusters acting as physically cross-linked sites. In the earlier stage, the resistance of clusters to the dissociation mainly caused the increase of the stress. While at larger strains, the soar of the stress was dominated by the stretching of bonds in the C-CL network. It was more difficult to dissociate clusters and stretch bonds with the physical interaction strength increasing. Clusters were broken up and frequently rejoined at lower rates, along with the slight bond stretching. Generally, this work provided the evolution of microstructure in hybrid DN gels, and guided the designing of high-performance polymers.

1. Introduction

The double network (DN) structure [1–6] exhibiting high strength and toughness gains increasing interest in the past two decades. Gong et al. [1] first fabricated the DN gel, and Gong [5] summarized design principles to prepare DN gels with superior mechanical properties. Following that, plenty of other DN gels such as the microgel-reinforced DN gel [7], ultrathin DN gel [4], free-shaped tough DN gel [8], and liquid crystalline DN gel [3] were developed afterward. Upon deformation, the first brittle and rigid network was fragmented into small clusters, which was the fundamental mechanism of the high toughness [2]. Therefore, the DN gel formed from the dual chemically cross-linked (C-CL) network could not recover.

To endow the DN gel with the self-healing ability, hybrid DN gels, where the first C-CL network was replaced by the physical interaction (PI) network cross linked through reversible interaction such as hydrogen bonds [9–12] ionic bonds [13–17], or hydrophobic association [18,19] were developed. These gels have comparable mechanical properties to conventional DN gels. Sun et al. [13] reported a hybrid DN gel, where the first network was the ionically cross-linked alginate. The synthetic hydrogel exhibited extreme stretchability (more than 20 times its original length) and high toughness (~9000 J/m^2). Since reversible bonds can break and reform, the deformation behavior of the hybrid DN gel is unique. During the deformation, ionic cross-links unzipped progressively while the C-CL network bridged the crack to maintain the integrity of the gel [13,14,16]. When loads were removed, the re-zipping of ionic crosslinks could be taken advantage to heal the damage. Chen et al. [9–11] prepared the agar/polyacrylamide (PAAm) hybrid DN gel, and they first proposed a chain pulling-out model, based on successive cyclic loading-unloading experiments, to account for the continuous fracture of the agar network. Agar chains began to unzip and pull out from physical associations at small strains far below the yielding, and this behavior could last over the whole tensile deformation. At the same time, there was no chain scission of the agar network, unlike the dual C-CL DN gel. Consequently, the elastic modulus declined, and the dissipation energy increased as the maximum strain increased. Many other papers adopted this model to interpret the enhancement mechanism of hybrid DN gels [15,17,20]. At larger strains, the stress was transferred to the C-CL network. As a result, the C-CL bonds broke, and the gel showed macroscopic destruction [16]. Furthermore, Lin et al. [20] presented a chain pulling-in model to account for the excellent compressibility of the agar/PAAm DN gel. Due to the finite lifetime of

* Corresponding author.
** Corresponding author.
E-mail addresses: wyu@ustc.edu.cn (Y. Wang), gongxl@ustc.edu.cn (X. Gong).

https://doi.org/10.1016/j.polymer.2020.122995
Received 24 July 2020; Received in revised form 28 August 2020; Accepted 30 August 2020
Available online 3 September 2020
0032-3861/

reversible bonds, the property of the PI network was sensitive to the strain rate, which led to rate-dependent behaviors of hybrid DN gels [10,12,15]. Wu et al. [12] studied the dependence of modulus on the strain rate. The dependence was concerned with the number of unrelaxed reversible bonds. More reversible bonds could not relax at higher strain rates. Besides, reversible bonds were easier to break at larger deformation, leading to the weaker dependence on rates at larger strains. Chen et al. [10] found more pronounced chain pulling-out behavior at lower strain rates.

Although the molecular model describing the destruction of the hybrid DN gel was presented, neither the unzipping nor the chain pulling-out was directly evidenced. Understandings of the evolution of microstructures in the hybrid DN gel still lacks. Molecular dynamics (MD) simulation is a technology to study the time evolution of the interacting particular system and predict the related physical properties. The motion of particles is governed by the classical Newton's equation. MD simulations can aid to construct the constitutive model [21,22] and provide a microscopic perspective of investigating polymers. Jang et al. [23] shed light on mechanical properties of the PEO-PAA DN gel by employing MD simulations. However, the all-atom level simulation constricted the number of atoms in the model. Zhang Liqun's group [24] tuned the mechanical performance of the DN elastomer by adjusting the stiffness of the stiff network, and furthermore they revealed the fracture mechanism on the coarse-grained (CG) level [25]. Gavrilov et al. [26] studied the phase behavior of the DN gel and its impact on mechanical properties by utilizing the dissipative particle dynamics method. However, the entanglement within the subnetwork was absent in this model. Higuchi et al. [27] performed CGMD simulations to elucidate the fracture process of the DN gels. Most studies [23,24,26–28] dealt with DN gels consisting of the double C-CL network. Simulations regarding hybrid DN gels are still scarce. Recently, Zhang et al. [29] created the CGMD model of the multi polymer network encompassing the hydrogen bond network, the coordination network, and the C-CL network to interpret toughing origins. Zhang et al. [30] successfully reproduced the higher peak stress of hybrid DN gels based on CGMD simulations. Nevertheless, the molecular mechanism of factors affecting the mechanical properties, such as the physical interaction strength, the number of interaction sites in PI networks, and the strain rate, remains elusive. Revealing the molecular origins of these parameters could further promote the mechanical performance.

This paper is organized as follows. In section 2, after describing the CGMD model representing the hybrid DN gel, the technique preparing initial configurations and elongating systems was explained. In section 3.1, we first tuned the physical interaction strength to construct the hybrid DN gel, and studied its influence on the structure and mechanical properties. Following that, the strain-rate effect of the hybrid DN gel was investigated in section 3.2. The effect of the number of PI sites was also studied and shown in the Supplementary data. At last, conclusions were drawn in section 4.

2. Models and simulation methods

In this study, the hybrid DN polymer represented by the CG model [31] was composed of 100 PI chains and 100 C-CL chains. The PI chain was made up of 20 repeating units (B_2AB_2) in which A-type beads could form physical interaction with each other. While C-CL chains only involved sequentially linked 100 C-type beads. C-CL bonds could be formed between C-type beads. All types of beads had the same mass m and diameter σ. Both PI chains and C-CL chains were illustrated in Fig. 1.

Herein, the Lennard-Jones (LJ) interaction [31] was utilized to model the non-bond potential between 2 beads separated by r_{ij}:

$$U_{ij}^{\mathrm{LJ}}(r_{ij}) = \begin{cases} 4\varepsilon_{ij}\left[\left(\frac{\sigma}{r_{ij}}\right)^{12} - \left(\frac{\sigma}{r_{ij}}\right)^{6}\right] + U_{\mathrm{cutoff}}, r_{ij} < r_c \\ 0 \qquad\qquad , r_{ij} \geq r_c \end{cases} \tag{1}$$

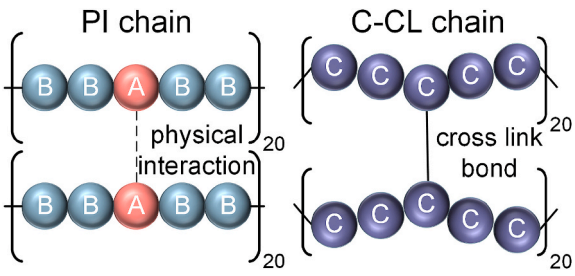

Fig. 1. Schematic representation of the PI chain where physical interaction could be formed among A-type beads, and the C-CL chain where C-type beads could be cross-linked by the covalent bond.

where U_{cutoff} is a constant term which makes sure the potential is continuous at the cutoff distance r_c. Reduced units were adopted here since the CGMD simulations here did not aim for the specified polymer. Therefore σ, m, and ε, which represented the units of length, mass, and energy, respectively, were all set to unity. The energy strength between beads i and$j$, that is ε_{ij}, apart from $\varepsilon_{\mathrm{AA}}$ was set to 1. The physical interaction strength was tailored by tuning $\varepsilon_{\mathrm{AA}}$ from 1 to 15 ($\varepsilon_{\mathrm{AA}} = 1, 3, 5, 10, 15$) when studying its effect. Zhang et al. [29,32], and Zanjani et al. [33] also employed the LJ potential to represent the reversible interaction. The FENE potential [31] was adopted to describe the connectivity of bonded beads:

$$U_{\mathrm{FENE}} = \begin{cases} -\frac{1}{2}kR_0^2 ln\left[1 - \left(\frac{r}{R_0}\right)^2\right], & r < R_0 \\ \infty \quad , & r \geq R_0 \end{cases}, \tag{2}$$

where the spring constant $k = 30\varepsilon/\sigma^2$ and the finite extended length $R_0 = 1.5\sigma$ could guarantee the stiffness of chains while avoid high-frequency modes and chains crossing.

Preparing the initial configuration of hybrid DN gels involved 2 steps.

Step 1. (cross-linking of C-CL chains): All chains were first placed randomly into a large box with the initial density $0.3\mathrm{m}/\sigma^3$ to free from the overlapping of chains. The simulation box was then compressed under the NPT ensemble with the reduced pressure $P^* = 1.0$ and the reduced temperature $T^* = 1.0$ to mix PI chains and C-CL chains. Density, potential, and the radius of gyration were checked to ensure the structure in equilibrium. After the equilibration, interchain cross-linking bonds were introduced into C-CL chains every 100 steps when any two C-type beads were within 1.0σ. The maximum number of bonds in each C-type bead was taken as 3. Since C-CL chains were loosely cross-linked in experiments [9,10,17], the number of cross-linking bonds was fixed at 1059, which corresponded to the cross-linking degree $\phi = 9.66\%$ ($\phi = N_c/N_t$ where N_c is the number of cross-linking bonds and N_t is the number of total bonds in C-CL chains). Noting that in order to achieve a homogenous mixing of PI chains and C-CL chains, $r_c = 2^{1/6}\sigma$ was chosen for beads belonging to same types of chains except for r_c^{AA} and others were set as $r_c = 2.5\sigma$. In addition, $\varepsilon_{\mathrm{AA}}$ was 1.0 before the cross linking so that the C-CL network was first set up. The frequency distribution of the number of cross-linking bonds between C-CL chains was given in Fig. S1(a). Considering the total number of cross-linking bonds, the C-CL network would be homogeneous if each C-CL chain cross linked with others with 21 bonds. The peak of the frequency occurred when the number of cross-linking bonds was 17 or 21, which were close. The heterogeneity in the network was also observed in experiments. Additionally, the snapshot of the cross-linking C-type beads in the model with $\varepsilon_{\mathrm{AA}} = 10$ was shown in Fig. S1(b). After cross-linking, all C-CL chains were linked together.

Step 2. (Constructing the PI network): After setting up the C-CL network, the system underwent a long period of relaxation in which thermodynamic statistics (temperature, density, and potential), as well as the radius of gyration almost did not fluctuate with the time. In this stage, all r_c were changed to 2.5σ to avoid the negative thermal expansion coefficient [34,35] and ε_{AA} was turned on. In other words, the PI network was constructed after the completion of the C-CL network. Wan et al. also changed r_c after cross-linking to mix the stiff and flexible chains homogeneously [24]. All parameters of Eq. (1) were listed in Table 1. The final configuration was selected as the initial configuration of the elongation, and it was also followed by the NVT production run at the same temperature. All simulations were carried out by the velocity Verlet algorithm with a time step of 0.001. The periodic boundary conditions, which were widely used in other literature [25,32] studying the DN structure, were applied along with all three directions of the simulation box. During the simulation, the temperature and pressure were controlled by the Nose–Hoover thermostat and Andersen barostat, respectively.

The tension simulation was performed in the NVT ensemble by elongating the simulation box in the z-direction with a constant engineering strain rate $0.0327/\tau$. The deformation was conducted every 1000 steps, as did in many previous studies [36,37]. The volume of the box was maintained, that is, the system was incompressible, so the Poisson's ratio was 0.5. Therefore, the stress in the tensional direction was evaluated as $\sigma = \sigma_{zz} - \frac{1}{2}(\sigma_{xx} + \sigma_{yy})$, where σ_{xx}, σ_{yy} and σ_{zz} were the normal stresses of the x-, y- and z-directions, respectively. The stress was calculated via the virial theorem [38]:

$$\sigma_{\alpha\beta} = \frac{1}{V}\left[\sum_{i=1}^{n} m_i v_{i\alpha} v_{i\beta} + \sum_{i=1}^{n-1}\sum_{j=i+1}^{n} r_{ij\alpha} F_{ij\beta}\right], \quad (3)$$

where m_i, $v_{i\alpha}$ and $v_{i\beta}$ are the mass and α- and β-component velocities of the bead i, respectively. And $r_{ij\alpha}$ and $F_{ij\beta}$ are the α-component distance and β-component force between bead i and j, respectively. V and n are the volume of the simulation box and the total number of atoms, respectively. When investigating the strain rate effect, we chose $0.00005/\tau$, $0.0001/\tau$, $0.000327/\tau$, $0.000654/\tau$, $0.00327/\tau$, and $0.0327/\tau$. The reproductivity of the data was validated by conducting 3 different deformation runs, starting from different equilibrium configurations at a given set of parameters. The commercial software J-OCTA 4.1 platform (JSOL Corporation, Japan) [39] was used to set up the model and visualize snapshots, and simulations were carried out by using COGNAC 9.2 [40].

Table 1
The parameters of Eq. (1).

Non-bond pair	$\varepsilon_{ij}/\varepsilon$	r_c/σ
A-A	1.0 (Step 1) 1.0, 3.0, 5.0,10.0, 15.0 (Step 2, loading step)	2.5
A-B	1.0	$2^{1/6}$ (Step 1) 2.5 (Step 2, loading step)
A-C	1.0	2.5
B–B	1.0	$2^{1/6}$ (Step 1) 2.5 (Step 2, loading step)
B–C	1.0	2.5
C–C	1.0	$2^{1/6}$ (Step 1) 2.5 (Step 2, loading step)

3. Results and discussion

3.1. Influence of the physical interaction strength ε_{AA}

The structure of hybrid DN gels was first studied by using pair distribution functions (PDFs) [41]. PDFs of the model with $\varepsilon_{AA} = 10$ were displayed in Fig. 2(a), while others were shown in Fig. S2. It could be clearly observed that the short-ranged peak of $g(r)_{A-A}$ was higher than those of other PDFs when $\varepsilon_{AA} > 1$, which indicated that A-type beads packed compactly with respect to other bead pairs. $g(r)_{A-A}$ with all ε_{AA} were compared in Fig. 2(b). The first peak of $g(r)_{A-A}$ increased with ε_{AA} increasing, which indicated the closer packing of A-type beads in models with higher ε_{AA}. What's more, there was only one peak of $g(r)_{A-A}$ at $r \sim 2\sigma$ when $\varepsilon_{AA} < 5$. Two peaks were found when $\varepsilon_{AA} \geq 5$, since dense clusters were formed by the compacted A-type beads. The aggregation shortened the distance between A-type beads, and the illustration of the dense clusters could be seen in Fig. 2(c). The arrangements of A-type beads in models with $\varepsilon_{AA} \leq 3$ were also drawn as a comparison. The apparent first peak and double peaks around $r \sim 2\sigma$ at high physical interaction strength were also observed in the work of Zhang et al. [32]

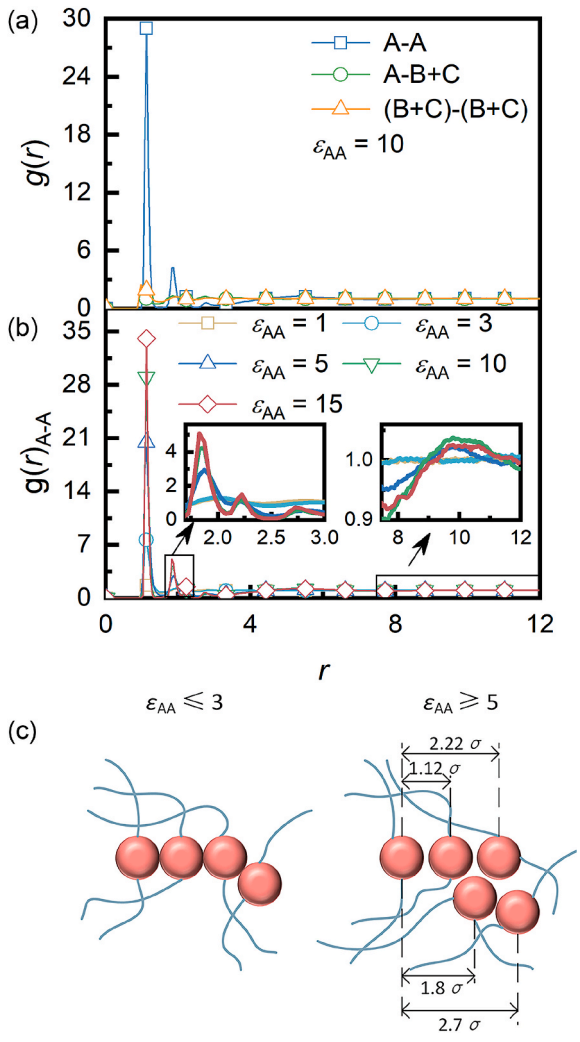

Fig. 2. (a) PDFs of the model with $\varepsilon_{AA} = 10$. (b) $g(r)_{A-A}$ for various ε_{AA}. Insets are the local enlarged drawings. (c) Schematic representation of the arrangement of A-type beads in the equilibrium state. The pink beads denoted A-type beads while the blue lines represented the other part of the PI chain. (For interpretation of the references to color in this figure legend, the reader is referred to the Web version of this article.)

In addition, the coordination number of A-type beads reached a threshold at $\varepsilon_{AA} = 5$ (Fig. S3), which further proved that the dense clusters exhibited in these models. Furtherly, the shallow peaks at $r \sim 10\sigma$ of $g(r)_{A-A}$ when $\varepsilon_{AA} \geq 5$ suggested the average separation distance of dense clusters. However, no long-range peaks were observed in models with $\varepsilon_{AA} \leq 3$, since A-type beads were distributed more uniformly in the simulation box. Next, the connectivity of clusters was characterized. Two A-type beads belonged to the same cluster when the distance was less than 1.5σ (the first valley of $g(r)_{A-A}$). Fig. 3(a) showed the normalized average number of clusters (NANC), $N_{clus}/\ N_A$ where N_{clus} is the average number of A-type beads. The NANC decreased quickly as ε_{AA} increased at first. When $\varepsilon_{AA} \geq 5$, the NANC tended to stable. The transition was also attributed to the dense clusters. The frequency distribution of the cluster size (the number of A-type beads contained in the cluster) was shown in Fig. S4. The peaks occurred at 2, 2, 10, 10 and 10 for the model with ε_{AA} from 1 to 15, respectively, which also demonstrated the formation of dense clusters. The dense clusters could be evidently observed by snapshots. Fig. 3(b and c) presented snapshots of the model with $\varepsilon_{AA} = 1$ and $\varepsilon_{AA} = 15$, where different colors of spheres represented A-type beads belonging to diverse clusters. Lines denoted B-type beads in the PI network. A-type beads in the model with $\varepsilon_{AA} = 1$ were distributed evenly (Fig. 3(b)), but they were trapped in clusters when $\varepsilon_{AA} = 15$ (Fig. 3(c)). Remarking that even if ε_{AA} became so high, A-type beads were not all connected. In other words, they did not locate in the same cluster. These clusters acted as cross-linked sites linking PI chains. Above all, the PI network, as well as the hybrid DN structure, were set up successfully when $\varepsilon_{AA} \geq 5$.

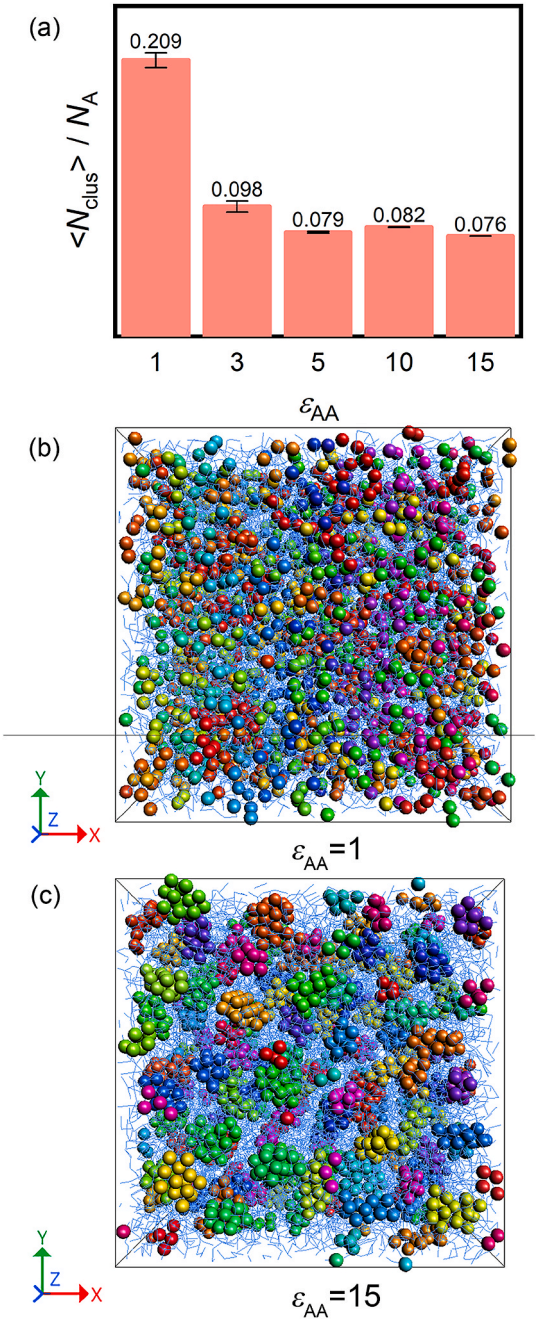

Fig. 3. (a) The NANC for models with various ε_{AA}. Snapshots of the model with (b) $\varepsilon_{AA} = 1$ and (c) $\varepsilon_{AA} = 15$, where different colors of spheres represented A-type beads belonging to diverse clusters. Lines denoted B-type beads in the PI network. To be more visually, the C-CL network was not shown. (For interpretation of the references to color in this figure legend, the reader is referred to the Web version of this article.)

After the structure was characterized, tensile simulations with different ε_{AA} were conducted. It was found in Fig. 4(a) that the stress underwent 3 stages: fast growth (I), strain softening (II), and strain hardening (III) for models with the DN structure. Feng et al. [42] synthesized a hybrid DN gel where the PI network was the thermoplastic polyurethane, and the C-CL network was the PAAm. The stress of the as-prepared gel also showed a first quick increase, followed by slow growth, and at last it increased rapidly. The similar trend was also observed in stress-strain curves found in other experiments [10,11,14,43,44], and the simulation [32]. The stress was independent of ε_{AA} when no PI network exhibited ($\varepsilon_{AA} \leq 3$). Nevertheless, it was promoted a great with ε_{AA} increasing if the DN structure was formed ($\varepsilon_{AA} \geq 5$). The hybrid DN gel, consisting of Fe^{3+} ionically cross-linked pectin and C-CL PAAm, developed by Lu et al. possessed higher stress than that of the PAAm single gel [14]. In addition, much literature confirmed the promotion of the stress in the hybrid DN gel than that of the single network gel [15,17,20]. Fig. 4(b) presented the bond stress and non-bond stress, which corresponded to the bond potential part and non-bond potential part of the second term of Eq. (3), respectively. Later, stress-strain curves of models with the DN structure ($\varepsilon_{AA} \geq 5$) would be discussed.

At stage I, the non-bond stress rose rapidly. To find out the network responsible for the growth of the non-bond stress, we took the model with $\varepsilon_{AA} = 5$ as an example to calculate the variation of the non-bond potential $\Delta E_{non-bond}$ for all bead pairs. $\Delta E_{non-bond}$ was defined as the difference of the non-bond energy between the tensile and initial states. As shown in Fig. S5$\Delta E^{AA}_{non-bond}$, the difference of the non-bond energy between A-type beads, increased sharply in stage I, which indicated that dense clusters adsorbed a large amount of energy obtained from the external force. The number of A-type beads in the range of $[r_1, r_2]$ from an A-type bead was calculated to reveal the evolution of clusters further. The definition was similar to the coordination number [36]:

$$PA = \frac{4\pi N_A}{V} \int_{r_1}^{r_2} r^2 g(r)_{A-A} dr, \tag{4}$$

where N_A, V and r are the number of A-type beads, the volume of the system, and the distance between two A-type beads, respectively. r_1 and r_2 are two successive minimums of $g(r)_{A-A}$. We counted A-type beads in the first three layers. Thus, for models with $\varepsilon_{AA} \leq 3$, $[r_1, r_2]$ were taken as $[0, 1.525\sigma]$, $[1.525\sigma, 2.475\sigma]$, and $[2.475\sigma, 3.425\sigma]$, respectively. These regions surrounded the first three peaks of $g(r)_{A-A}$, respectively. Similarly, $[r_1, r_2]$ for models with $\varepsilon_{AA} \geq 5$ were chosen as $[0, 1.525\sigma]$, $[1.525\sigma, 2.575\sigma]$, and $[2.575\sigma, 3.175\sigma]$, respectively. The number of A-type beads in the first three layers were defined as PA1, PA2, and PA3, respectively (Fig. 5(a–c)). In stage I, PA1 and PA3 owned a short plateau, then PA1 declined, but PA3 went up. It suggested that dense clusters remained stable initially. Then A-type beads in the first layer were pulled out to the second layer, which squeezed out A-type beads in the

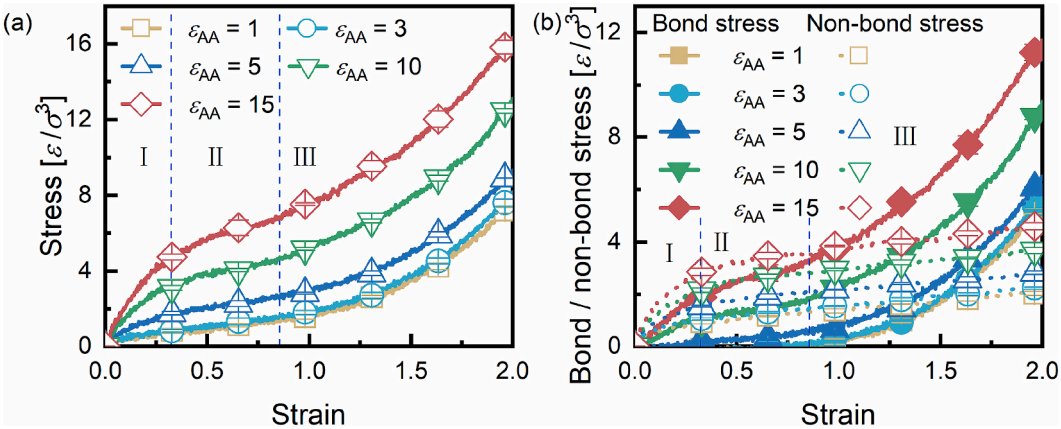

Fig. 4. The (a) stress, (b) bond stress, and non-bond stress as a function of strain for various ε_{AA}.

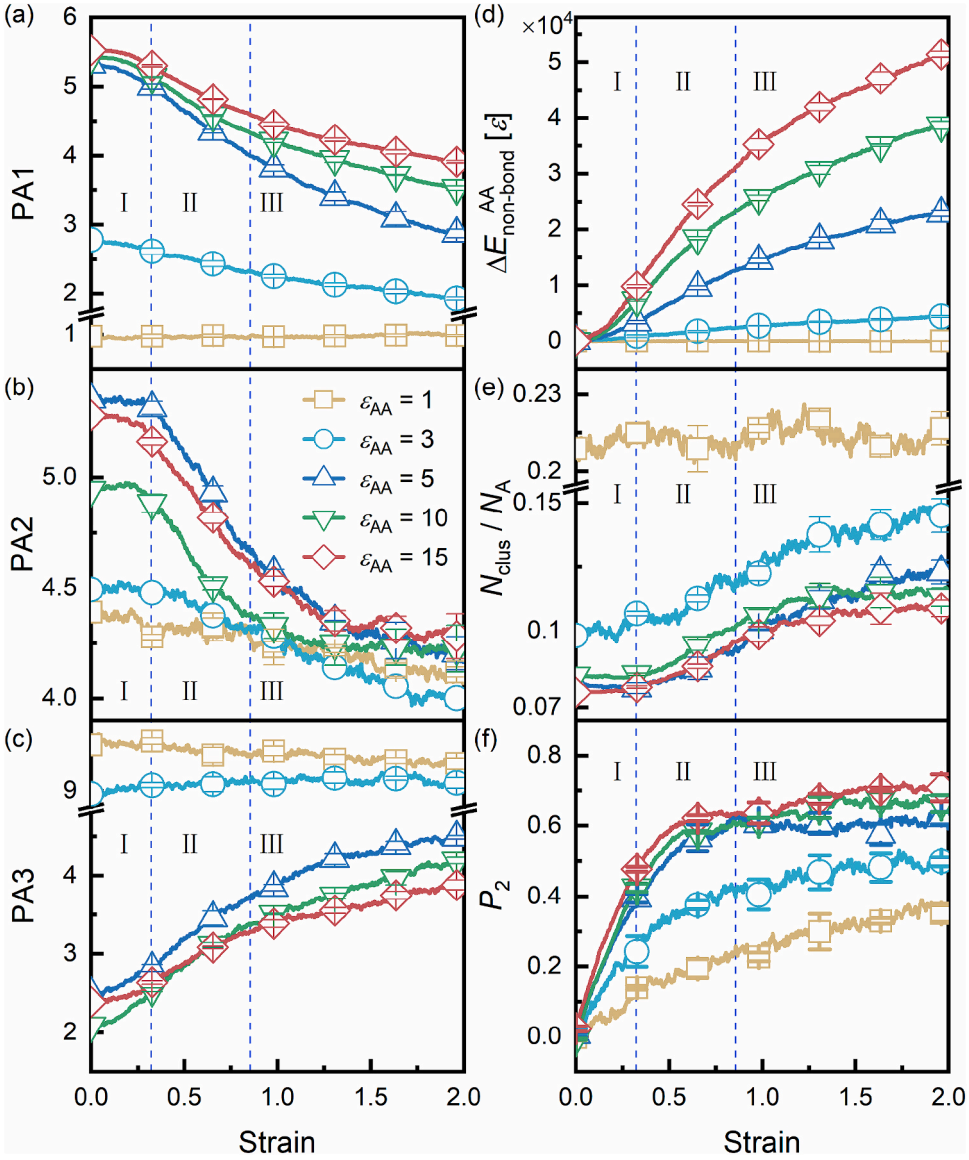

Fig. 5. (a) PA1, (b) PA2, (c) PA3, (d) variations of the non-bond energy between A-type beads, (e) NNC, and (f) P_2 as a function of strain for various ε_{AA}.

second layer into the third layer. As a result, PA2 remained stable in this stage. In this region, A-type beads started to separate apart from each other, which led to the increase of $\Delta E^{AA}_{non-bond}$ (Fig. 5(d)). The separated A-type beads, driving B-type beads through the covalent bond, diffused into the C-CL network gradually, indicated by the decrease of $\Delta E^{AC}_{non-bond}$ and $\Delta E^{BC}_{non-bond}$ (Fig. S5). Moreover, the normalized number of clusters (NNC), N_{clus}/N_A, was depicted in Fig. 5(e). In this stage, NNC did not change with the strain, revealing that dense clusters just became loose but did not dissociate. Then, the orientation of clusters was evaluated by adopting the second Legendre polynomial P_2:

$$P_2 = \frac{1}{2}\left(3\cos^2\theta - 1\right), \tag{5}$$

where θ represents the angle between the first principle inertia axis of the cluster and the tensile axis, and the bracket denotes the average among all clusters. P_2 takes the value of −0.5, 0, or 1 when the two axes are perpendicular, disordered, or parallel, respectively. As shown in Fig. 5(f), P_2 increased soon with strain increasing in this stage, which suggested that clusters also accommodated the deformation by aligning themselves to the tensile direction. Therefore, a larger force, which led to the increase of non-bond stress, was required to orient clusters and separate A-type beads in the originally dense cluster under tensile strains. Compared to the non-bond stress, the bond stress showed slow growth. The bond energy of the C-CL network and the PI network were shown in Fig. 6. The bond energy of the PI network changed greatly with respect to that of the C-CL network, indicating that bonds of PI chains stretched more. In order to make clear which type of bond in PI chains being responsible for the increase, the mean bond energy, normalized by the number of bonds, of each bond type in PI chains was shown in Fig. S6. The mean bond energy of B–B bonds grew fast in this stage with respect to that of A-B bonds. As shown in Fig. S7, the density of A-type beads was concentrated in clusters, while B-type beads dispersed more uniformly. Consequently, the local density around clusters was higher than that in other parts. The higher local density around clusters indicated stronger attraction, resulting in slighter deformation of A-B bonds.

In the strain softening region (stage II), the non-bond stress tended to maintain its level. $\Delta E^{AA}_{non-bond}$ still took up the major part (Fig. S5). In Fig. 5(a–c), PA1, and PA2 dropped off soon, whereas PA3 increased quickly. These indicated the severe separation of A-type beads. The aggregation of A-type beads furtherly decreased, which accounted for the dramatic increase of $\Delta E^{AA}_{non-bond}$ (Fig. 5(d)). The NNC also increased sharply in this stage, meaning the dissociation of clusters, shown in Fig. 5(e). After stage I, clusters could barely bear loads, since they had become loose. Thus, they were broken up under further deformation, impeding the rise of the non-bond stress. As clusters were destroyed, P_2 in Fig. 5(f) tended to rise slowly in this region. Besides, from Fig. 6, the bond energy of the C-CL network started to increase, while that of the PI network reached a plateau. Owing to the stretching of bonds in the C-CL network, the increase of the bond stress accelerated. To conclude, both the C-CL and PI network contributed to the stress, in which the C-CL network began to get tensed, and the PI network was broken up in this stage. The competition between the bond and non-bond stress led to the strain softening.

At last, for the strain hardening stage (stage III) in Fig. 5(a–c), PA1, and PA2 decreased a little slowly since A-type beads were far away from each other. The NNC and $\Delta E^{AA}_{non-bond}$ increased slowly, since many clusters had been broken up. There were few large clusters which could bear the stress. Additionally, the bond energy of the C-CL network increased notably with regard to that of the PI network. So the bond stretching of the C-CL network took a prominent role in improving the bond stress. Hence, the remarkable stretching of the C-CL network and the further dissociation of clusters made the bond stress overtake the non-bond stress, and lead to the soar of the bond stress. This remarkable increase caused the strain hardening.

As mentioned above, the growth of the stress was originated from the resistance of clusters to dissociation and bonds to stretching. Herein, the influence of ε_{AA} would be discussed. When there was only the C-CL network ($\varepsilon_{AA} = 1$ or 3), PA3 was the largest, as shown in Fig. 5(a–c). Since A-type beads were evenly distributed, more A-type beads exhibited in the farther region. And PA1, PA2, and PA3 varied slowly due to the uniform distribution of A-type beads. On the contrary, dense clusters were formed once the DN structure was formed. A-type beads prevailed in the first and the second layer. PA1, PA2, and PA3 changed a great. The PA1 exhibited an increasing trend as ε_{AA} increased, which revealed that clusters were more compact at higher ε_{AA}. As shown in Fig. 5(d), $\Delta E^{AA}_{non-bond}$ increased with the growth of ε_{AA}. The increase related to the separation of A-type beads, as discussed above. As ε_{AA} increased, A-type beads got closer together, which required larger force to separate. Hence, the stress was more concentrated on clusters when ε_{AA} was high, which led to higher P_2 (Fig. 5(f)). Therefore, the resistance of clusters to dissociation was improved with ε_{AA} increasing, which led to higher non-bond stress. In Fig. 6, both the bond energy of the C-CL and PI network rose with the increase of ε_{AA}. The weaker relaxation of chains due to larger intermolecular attraction made the system difficult to stretch. Thus the stronger force was needed to elongate the model to the same strain, which led to the apparent bond stretching.

3.2. Influence of the strain rate

After investigating the effect of ε_{AA}, the model with the hybrid DN structure ($\varepsilon_{AA} = 5$) was chosen to study the rate-dependent behavior. Stress-strain curves with various stain rates were shown in Fig. 7(a). The

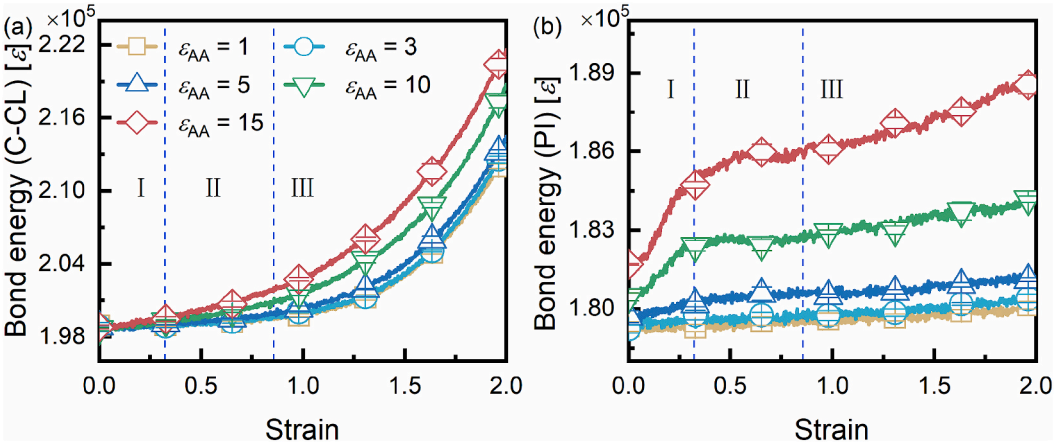

Fig. 6. The bond energy of the (a) C-CL network and (b) PI network as a function of strain for various ε_{AA}.

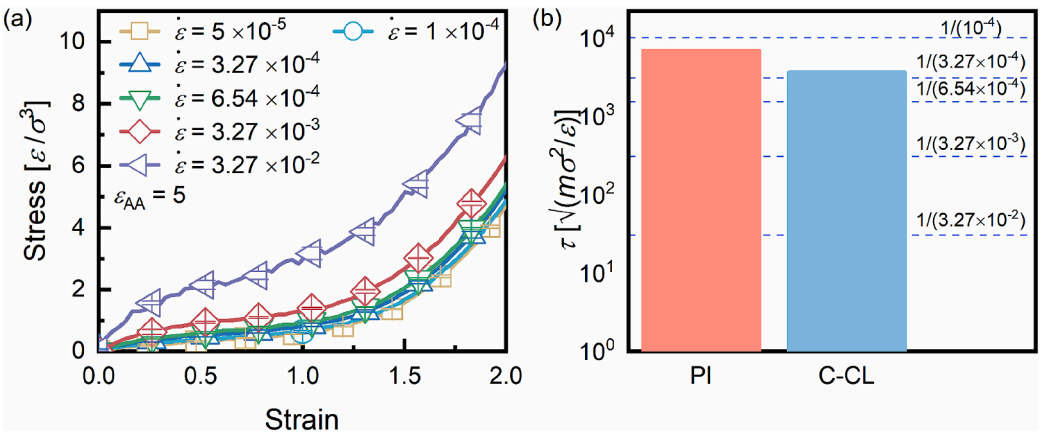

Fig. 7. (a) The stress-strain curves of the model with $\varepsilon_{AA} = 5$ at various strain rates. (b) The relaxation time of PI and C-CL chains for the model with $\varepsilon_{AA} = 5$. The blue dashed lines denoted the time scales of strain rates. (For interpretation of the references to color in this figure legend, the reader is referred to the Web version of this article.)

system exhibited obvious strain-rate sensitivity when the strain rate was above $1 \times 10^{-4}/\tau$. The stress was promoted when increasing the strain rate. This rate-dependent effect of the stress was also found in the hybrid PAAm/agar gels [10] and the hybrid DN elastomer [12]. Many reports [45–47] attributed the strain rate effect to the mismatch between the relaxation time of the polymer and the loading time. If the loading speed was faster, polymer chains could not relax to disentangle. They behaved like stiff solids. In contrast, the polymer would become viscous liquids with shorter relaxation time. Herein, the relaxation time τ, which measured the time required for monomers or chains to move to the distance corresponding to their own size, was inversely proportional to the diffusion coefficient D. D was calculated from the Einstein's equation:

$$D = \lim_{t\to\infty} \frac{1}{6t} \mathrm{MSD(t)} \sim \frac{1}{\tau} \tag{6}$$

where MSD is the mean-square displacement. It could be found in Fig. 7 (b) that from $3.27 \times 10^{-4}/\tau$, the relaxation time of both the PI and C-CL chains exceeded the time scale of the loading. Increasing the strain rate would delay the relaxation of chains, which led to higher stress. Besides, the relaxation time of PI chains was longer than that of C-CL chains. Thus, the PI network behaved as the hard phase, providing the initial modulus under the deformation. This was also in agreement with the conclusion drawn in section 3.1 that the PI network was responsible for the fast growth (stage I) of the stress. The hybrid DN gel was similar to the conventional soft-hard phase polymer, like polyurethane whose Young's modulus increased as hard segment content rose (Fig. S8) [48–50].

As shown in Fig. 7(a), the stress quickly passed through the rapid growth stage and entered into the strain softening region when the strain rate was low. While with a higher strain rate, the first stage was prolonged. The stress in the first stage was mainly concerned with the resistance of clusters to the deformation. The NNC, $\Delta E^{AA}_{non-bond}$, and P_2 for all strain rates were presented in Fig. 8. The NNC and $\Delta E^{AA}_{non-bond}$ decreased first with the strain when the loading time exceeded the relaxation time ($5 \times 10^{-5}/\tau$ and $1 \times 10^{-4}/\tau$). Since PI chains were relaxed at these rates, clusters were broken up easily. The A-type beads escaping from the original clusters could take part in other clusters. When one cluster was totally destructed, and the released A-type beads joined another cluster, the NNC and $\Delta E^{AA}_{non-bond}$ would decline. The easy dissociation of clusters would shorten the first stage of the stress. With the development of the strain, the distance between A-type beads got farther, which prevented the lonely A-type beads from entering into another cluster. So the NNC and $\Delta E^{AA}_{non-bond}$ increased again at large strains. Once the strain rate was high, the NNC remained stable for all

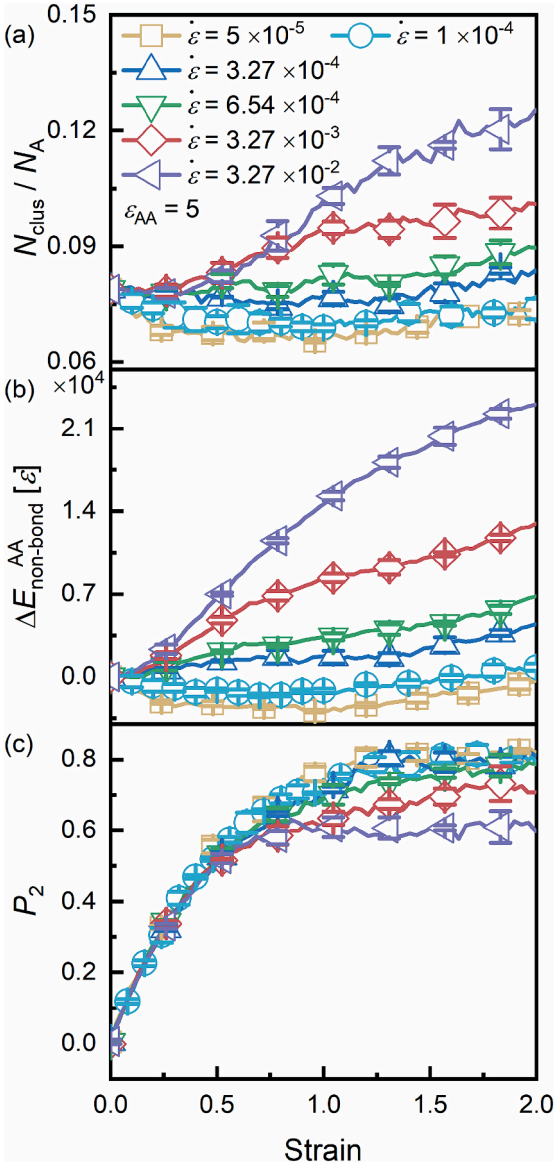

Fig. 8. (a) The NNC, (b) variations of the non-bond energy between A-type beads and (c) P_2 as a function of strain for the model with various strain rates.

rates at the first stage due to the stiff clusters, which were hard to break. The $\Delta E^{AA}_{non-bond}$ increased with increasing rates, suggesting that more energy was required to make clusters loose. The stiffer clusters at higher rates guaranteed the longer first stage of the stress as well as its higher level. After stage I, the NNC began to increase, which indicated clusters were broken up. With a higher rate, the dynamics of the polymer was slowed down, so it was difficult for the escaped A-type beads to rejoin the cluster, resulting in the growing NNC with the strain rate. In addition,P_2 decreased as the strain rate rose, which arose from the "frozen" A-type beads at higher rates.

To evidently observe the influence of the strain rate on the evolution of clusters, 3 clusters among all clusters were selected, as shown in Fig. 9 (a and b). Snapshots of these clusters as well as the chains with which the 3 clusters linked when $\dot{\varepsilon} = 5 \times 10^{-5}/\tau$ and $\dot{\varepsilon} = 0.0327/\tau$ were displayed in Fig. 9(b–h). At a lower strain rate ($5 \times 10^{-5}/\tau$), beads could hop to neighbor clusters, which efficiently dissipated the energy. For example, the blue bead marked by the arrow jumped from cluster 2 to cluster 1 at the strain of 0.06. And red beads in cluster 1 hopped to cluster 2 and cluster 3 when the strain was 0.09. Keeping increasing the strain would destroy clusters, which was seen at the strain of 1.05. The originally integrated clusters were broken up. If the system was loaded with a higher rate, clusters seemed to be "frozen". Clusters still remained intact even at the strain of 0.32, which was the end of the rapid growth stage. But clusters became loose and aligned themselves to the z-direction. Beads began to get out from clusters when the strain was 0.59, which was much larger than 0.06 at lower rates. Compared to the system with a lower rate at the same strain of 1.05, clusters showed less dissociation at higher rates. The continuous destruction of clusters coincided with the chain pulling-out model [10]. The purple chain was gradually pulled out from cluster 3 as cluster 3 was broken up into many sub-clusters. Its pulling-out was originated from separating the green bead marked by the green arrow from cluster 3. The pulling-out occurred just at the strain of 0.09 with the lower rate, but at the strain of 0.59 in the higher rate. So the pulling-out of chains happened earlier and easier at lower rates. Concerned with discussion in Fig. 8(a), the dissociation of clusters indicated the PI chains pulled out from clusters. The easy disruption of clusters at lower rates meant the pulling-out became frequent, which was the same as the chain pulling-out model [10]. The pulling-out behaviors turn evident, as suggested by the earlier and larger hysteresis.

It could be observed from Fig. 7(a) that the modulus in the stress softening region increased with the increase of the strain rate. According to section 3.1, the enhancement of modulus in this stage was originated from the tenseness of the network. The bond energy of the C-CL and PI network were shown in Fig. 10. The bond energy of both the network

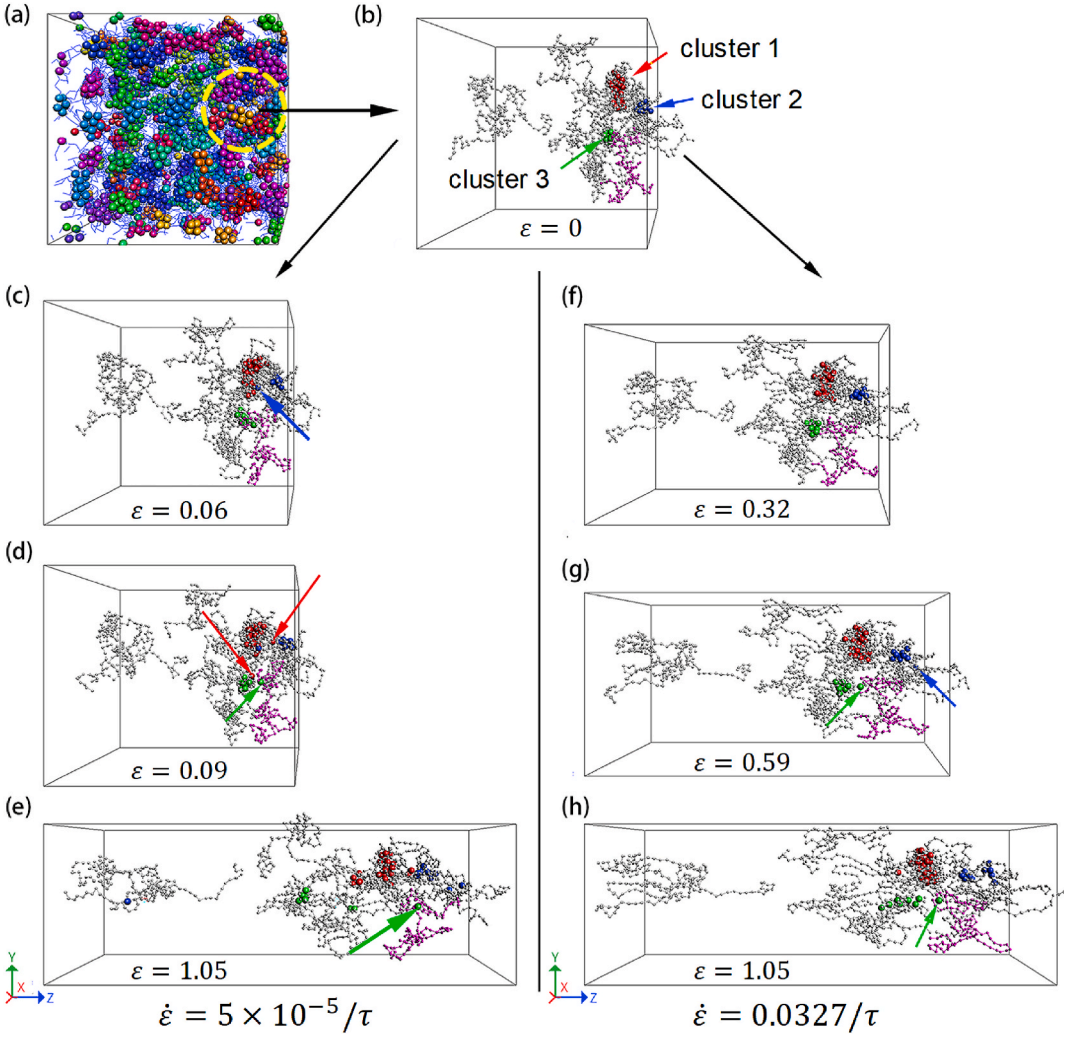

Fig. 9. (a) Snapshot of the model with $\varepsilon_{AA} = 5$ where different colors of spheres represented A-type beads belonging to diverse clusters. Lines denoted B-type beads in the PI network. (b–h) The evolution of 3 clusters circled in (a) as well as chains with which the clusters linked when (c–e) $\dot{\varepsilon} = 5 \times 10^{-5}/\tau$ and (f–h) $\dot{\varepsilon} = 0.0327/\tau$. The red, blue, and green spheres represented A-type beads belonging to clusters 1, 2, and 3, respectively. The grey spheres denoted PI chains which clusters linked to, and the purple chain was a selected chain of them. Noting that, to clearly observe the clusters, the radii of grey and purple beads were reduced to 0.4 times of those of red, blue, and green spheres. (For interpretation of the references to color in this figure legend, the reader is referred to the Web version of this article.)

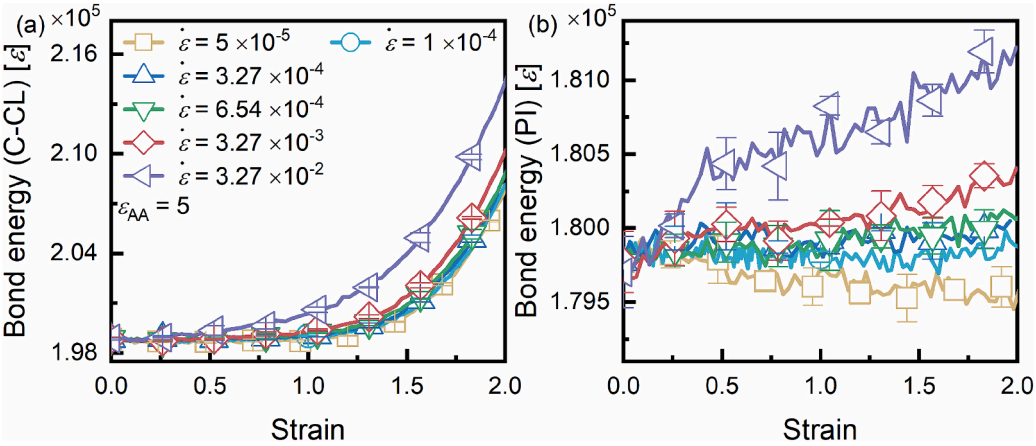

Fig. 10. The bond energy of the (a) C-CL network and (b) PI network as a function of strain for the model with various strain rates.

increased as rates went up. The higher the strain rate, the less the relaxation of the system, so the stronger the bond stretching was for both the network. Noting that for the strain rate of $5 \times 10^{-5}/\tau$, the bond energy of the PI network decreased in the whole strain range. At this rate, the PI network was fully relaxed, so the bond length shifted to the balanced state swiftly. In summary, with increasing strain rates, the clusters became stiffer, and the bond stretching was more evident.

4. Conclusion

In this work, hybrid DN gels consisting of the PI network and the C-CL network were reproduced by utilizing the CG model. The effect of the physical interaction strength ε_{AA} was first studied. When $\varepsilon_{AA} \geq 5$, PI chains were cross linked through clusters aggregated by A-type beads. The tensile stress-strain curves contained 3 regions: the rapid growth region was followed by the strain softening and then hardening regions. The first region was concerned with the orientation of clusters and the separation of A-type beads in clusters. After this, clusters dissociated, and the C-CL network began to get tensed. The competition between them caused the strain softening. The notable bond stretching in the C-CL network at larger strains contributed to the strain hardening. With the growth of ε_{AA}, more force was required to dissociate clusters and stretch bonds, leading to the higher stress. The hybrid DN gel exhibited rate sensitivity if its relaxation time was longer than the loading time. As the strain rate increased, clusters became stiffer, and the network got tenser. So it was more difficult to elongate the system. In conclusion, this work not only illuminated the molecular origins of the deformation, but also discussed the effect ofε_{AA} and the strain rate of hybrid DN gels.

Declaration of competing interest

The authors declare that they have no known competing financial interests or personal relationships that could have appeared to influence the work reported in this paper.

Acknowledgements

The authors acknowledge financial supports from the National Natural Science Foundation of China (Grant No. 11972337, 11772320) and the Strategic Priority Research Program of the Chinese Academy of Sciences (Grant No. XDB22040502) are gratefully acknowledged.

Appendix A. Supplementary data

Supplementary data to this article can be found online at https://doi.org/10.1016/j.polymer.2020.122995.

References

[1] J.P. Gong, Y. Katsuyama, T. Kurokawa, Y. Osada, Double-network hydrogels with extremely high mechanical strength, Adv. Mater. 15 (14) (2003) 1155–1158.
[2] Y.-H. Na, Y. Tanaka, Y. Kawauchi, H. Furukawa, T. Sumiyoshi, J.P. Gong, Y. Osada, Necking phenomenon of double-network gels, Macromolecules 39 (14) (2006) 4641–4645.
[3] W. Yang, H. Furukawa, J.P. Gong, Highly extensible double-network gels with self-assembling anisotropic structure, Adv. Mater. 20 (23) (2008) 4499–4503.
[4] S. Liang, Q.M. Yu, H. Yin, Z.L. Wu, T. Kurokawa, J.P. Gong, Ultrathin tough double network hydrogels showing adjustable muscle-like isometric force generation triggered by solvent, Chem. Commun. 48 (2009) 7518–7520.
[5] J.P. Gong, Why are double network hydrogels so tough? Soft Matter 6 (12) (2010) 2583–2590.
[6] T. Matsuda, R. Kawakami, R. Namba, T. Nakajima, J.P. Gong, Mechanoresponsive self-growing hydrogels inspired by muscle training, Science 363 (6426) (2019) 504–508.
[7] J. Hu, K. Hiwatashi, T. Kurokawa, S.M. Liang, Z.L. Wu, J.P. Gong, Microgel-reinforced hydrogel films with high mechanical strength and their visible mesoscale fracture structure, Macromolecules 44 (19) (2011) 7775–7781.
[8] T. Nakajima, N. Takedomi, T. Kurokawa, H. Furukawa, J.P. Gong, A facile method for synthesizing free-shaped and tough double network hydrogels using physically crosslinked poly (vinyl alcohol) as an internal mold, Polym. Chem. 1 (5) (2010) 693–697.
[9] Q. Chen, L. Zhu, C. Zhao, Q. Wang, J. Zheng, A robust, one-pot synthesis of highly mechanical and recoverable double network hydrogels using thermoreversible sol-gel polysaccharide, Adv. Mater. 25 (30) (2013) 4171–4176.
[10] Q. Chen, L. Zhu, L. Huang, H. Chen, K. Xu, Y. Tan, P. Wang, J. Zheng, Fracture of the physically cross-linked first network in hybrid double network hydrogels, Macromolecules 47 (6) (2014) 2140–2148.
[11] Q. Chen, D.D. Wei, H. Chen, L. Zhu, C.C. Jiao, G. Liu, L.N. Huang, J. Yang, L. B. Wang, J. Zheng, Simultaneous enhancement of stiffness and toughness in hybrid double-network hydrogels via the first, physically linked network, Macromolecules 48 (21) (2015) 8003–8010.
[12] J. Wu, L.-H. Cai, D.A. Weitz, Tough self-healing elastomers by molecular enforced integration of covalent and reversible networks, Adv. Mater. 29 (38) (2017) 1702616.
[13] J.-Y. Sun, X. Zhao, W.R.K. Illeperuma, O. Chaudhuri, K.H. Oh, D.J. Mooney, J. J. Vlassak, Z. Suo, Highly stretchable and tough hydrogels, Nature 489 (7414) (2012) 133–136.
[14] X. Lu, C.Y. Chan, K.I. Lee, P.F. Ng, B. Fei, J.H. Xin, J. Fu, Super-tough and thermo-healable hydrogel – promising for shape-memory absorbent fiber, J. Matter. Chem. B 2 (43) (2014) 7631–7638.
[15] S. Liu, L. Li, Recoverable and self-healing double network hydrogel based on κ-carrageenan, ACS Appl. Mater. Interfaces 8 (43) (2016) 29749–29758.
[16] X. Li, Y. Zhao, D. Li, G. Zhang, S. Long, H. Wang, Hybrid dual crosslinked polyacrylic acid hydrogels with ultrahigh mechanical strength, toughness and self-healing properties via soaking salt solution, Polymer 121 (2017) 55–63.
[17] R. Niu, Z. Qin, F. Ji, M. Xu, X. Tian, J. Li, F. Yao, Hybrid pectin–Fe3+/ polyacrylamide double network hydrogels with excellent strength, high stiffness, superior toughness and notch-insensitivity, Soft Matter 13 (48) (2017) 9237–9245.
[18] J. Chen, Y. Ao, T. Lin, X. Yang, J. Peng, W. Huang, J. Li, M. Zhai, High-toughness polyacrylamide gel containing hydrophobic crosslinking and its double network gel, Polymer 87 (2016) 73–80.
[19] F. Chen, Z. Tang, S. Lu, L. Zhu, Q. Wang, Q. Gang, J. Yang, Q. Chen, Fabrication and mechanical behaviors of novel supramolecular/polymer hybrid double network hydrogels, Polymer 168 (2019) 159–167.
[20] T. Lin, Q. Bai, J. Peng, L. Xu, J. Li, M. Zhai, One-step radiation synthesis of agarose/ polyacrylamide double-network hydrogel with extremely excellent mechanical properties, Carbohydr. Polymer 200 (2018) 72–81.

[21] Y. Li, S. Tang, M. Kroger, W.K. Liu, Molecular simulation guided constitutive modeling on finite strain viscoelasticity of elastomers, J. Mech. Phys. Solid. 88 (2016) 204–226.
[22] R. Unger, B. Arash, W. Exner, R. Rolfes, Effect of temperature on the viscoelastic damage behaviour of nanoparticle/epoxy nanocomposites: constitutive modelling and experimental validation, Polymer 191 (2020) 122265.
[23] S.S. Jang, W.A. Goddard, M.Y.S. Kalani, Mechanical and transport properties of the poly(ethylene oxide)−Poly(acrylic acid) double network hydrogel from molecular dynamic simulations, J. Phys. Chem. B 111 (7) (2007) 1729–1737.
[24] H. Wan, J. Shen, N. Gao, J. Liu, Y. Gao, L. Zhang, Tailoring the mechanical properties by molecular integration of flexible and stiff polymer networks, Soft Matter 14 (12) (2018) 2379–2390.
[25] H. Li, H. Wu, B. Li, Y. Gao, X. Zhao, L. Zhang, Molecular dynamics simulation of fracture mechanism in the double interpenetrated cross-linked polymer, Polymer 199 (2020) 122571.
[26] A.A. Gavrilov, P.I. Kos, A.V. Chertovich, Simulation of phase behavior and mechanical properties of ideal interpenetrating networks, Polym. Sci. 58 (6) (2016) 916–924.
[27] Y. Higuchi, K. Saito, T. Sakai, J.P. Gong, M. Kubo, Fracture process of double-network gels by coarse-grained molecular dynamics simulation, Macromolecules 51 (8) (2018) 3075–3087.
[28] K. Boudraa, T. Bouchaour, U. Maschke, Thermal analysis of interpenetrating polymer networks through molecular dynamics simulations: a comparison with experiments, J. Therm. Anal. Calorim. 140 (2020) 1845–1857.
[29] Z.Y. Zhang, J. Liu, S. Li, K. Gao, V. Ganesan, L.Q. Zhang, Constructing sacrificial multiple networks to toughen elastomer, Macromolecules 52 (11) (2019) 4154–4168.
[30] B.R. Zhang, J. Ke, J.R. Vakil, S.C. Cummings, Z.A. Digby, J.L. Sparks, Z.J. Ye, M. B. Zanjani, D. Konkolewicz, Dual-dynamic interpenetrated networks tuned through macromolecular architecture, Polym. Chem. 10 (46) (2019) 6290–6304.
[31] K. Kremer, G.S. Grest, Dynamics of entangled linear polymer melts: A molecular-dynamics simulation, J. Chem. Phys. 92 (8) (1990) 5057–5086.
[32] Z. Zhang, J. Liu, L. Zhang, Tuning the structure and mechanical properties of double-network elastomer: molecular dynamics simulation, Chin. Sci. Bull. 63 (34) (2018) 3631–3641.
[33] M.B. Zanjani, B. Zhang, B. Ahammed, J.P. Chamberlin, P. Chakma, D. Konkolewicz, Z. Ye, Computational investigation of the effect of network architecture on mechanical properties of dynamically cross-linked polymer materials, Macromol. Theory Simul. 28 (4) (2019) 1900008.
[34] M. Wolfgardt, J. Baschnagel, W. Paul, K. Binder, Entropy of glassy polymer melts: comparison between Gibbs-DiMarzio theory and simulation, Phys. Rev. E 54 (2) (1996) 1535–1543.
[35] M. Wolfgardt, K. Binder, On the equation of state for thermal polymer solutions and melts with attractive interaction, Macromol. Theory Simul. 5 (4) (1996) 699–712.
[36] N. Molinari, A.P. Sutton, A.A. Mostofi, Mechanisms of reinforcement in polymer nanocomposites, Phys. Chem. Chem. Phys. 20 (35) (2018) 23085–23094.
[37] N. Molinari, S. Angioletti-Uberti, Nanoparticle organization controls their potency as universal glues for gels, Nano Lett. 18 (6) (2018) 3530–3537.
[38] R. Clausius, XVI. On a mechanical theorem applicable to heat, The London, Edinburgh, and Dublin Philosophical Magazine and Journal of Science 40 (265) (1870) 122–127.
[39] J-OCTA (Accessed 8.4 2018), https://www.j-octa.com/.
[40] T. Aoyagi, F. Sawa, T. Shoji, H. Fukunaga, J.I. Takimoto, M. Doi, A general-purpose coarse-grained molecular dynamics program, Comput. Phys. Commun. 145 (2) (2002) 267–279.
[41] T. Aoyagi, COGNAC: coarse-grained molecular dynamics simulator, in: J.A.f. C. Innovation (Ed.), Computer Simulation of Polymeric Materials: Applications of the OCTA System, Singapore, 2016, pp. 29–65.
[42] F. Wu, L. Chen, Y. Wang, B. Fei, Tough and stretchy double-network hydrogels based on in situ interpenetration of polyacrylamide and physically cross-linked polyurethane, J. Mater. Sci. 54 (18) (2019) 12131–12144.
[43] Y. Yang, Z. Ye, X. Liu, J. Su, A healable waterborne polyurethane synergistically cross-linked by hydrogen bonds and covalent bonds for composite conductors, J. Mater. Chem. C 8 (15) (2020) 5280–5292.
[44] Q. Zhang, M. Wu, X. Hu, W. Lu, M. Wang, T. Li, Y. Zhao, A novel double-network, self-healing hydrogel based on hydrogen bonding and hydrophobic effect, Macromol. Chem. Phys. 221 (3) (2020) 1900320.
[45] S. Wang, W.Q. Jiang, W.F. Jiang, F. Ye, Y. Mao, S.H. Xuan, X.L. Gong, Multifunctional polymer composite with excellent shear stiffening performance and magnetorheological effect, J. Mater. Chem. C 2 (34) (2014) 7133–7140.
[46] Y. Wang, L. Ding, C. Zhao, S. Wang, S. Xuan, H. Jiang, X. Gong, A novel magnetorheological shear-stiffening elastomer with self-healing ability, Compos. Sci. Technol. 168 (2018) 303–311.
[47] X.-Z. Cao, H. Merlitz, C.-X. Wu, Mechanical strength management of polymer composites through tuning transient networks, J. Phys. Chem. Lett. 11 (3) (2020) 710–715.
[48] E. Ylgör, I. Ylgör, Hydrogen bonding: a critical parameter in designing silicone copolymers, Polymer 42 (19) (2001) 7953–7959.
[49] R.M. Versteegen, R. Kleppinger, R.P. Sijbesma, E.W. Meijer, Properties and morphology of segmented copoly(ether urea)s with uniform hard segments, Macromolecules 39 (2) (2006) 772–783.
[50] A. Arun, K.K.J. Baack, R.J. Gaymans, Polyurethane tri-block copolymers-synthesis, mechanical, elastic, and rheological properties, Polym. Eng. Sci. 50 (4) (2010) 747–755.